processes

MDPI

Article

Eco-Friendly Synthesis of TiO_2/ZIF-8 Composites: Characterization and Application for the Removal of Imidacloprid from Wastewater

Lucija Bogdan [1,*], Ana Palčić [2,*], Marina Duplančić [1], Mirela Leskovac [1] and Vesna Tomašić [1]

[1] Faculty of Chemical Engineering and Technology, University of Zagreb, Marulićev Trg 19, 10000 Zagreb, Croatia
[2] Institute Ruđer Bošković, Bijenička Cesta 54, 10000 Zagreb, Croatia
* Correspondence: lbogdan@fkit.hr (L.B.); ana.palcic@irb.hr (A.P.)

Abstract: The aim of this work was to develop hybrid TiO_2/ZIF-8 photocatalysts and test their activity for the removal of agricultural pollutants in water. The hybrid photocatalysts were prepared by an innovative method involving hydrothermal synthesis at 150 °C using a mechanochemically synthesized zeolitic imidazolate framework (ZIF-8) and titanium tetraisopropoxide as a titanium dioxide (TiO_2) precursor. Three composite photocatalysts with different mass fractions of titanium dioxide (5, 50, and 95 wt%) were synthesized and characterized, and their adsorption and photocatalytic properties investigated for the removal of imidacloprid. The equilibrium adsorption test showed that ZIF-8 is a good adsorbent and can adsorb 65% of the model component under the working conditions used in this work, while the hybrid photocatalysts can adsorb 1–3% of the model component. It is assumed that the adsorption is hindered by the TiO_2 layer on the surface of ZIF-8, which blocks the interactions of ZIF-8 and imidacloprid. A significant decrease in band gap energies (3.1–3.6 eV) was observed for the hybrid TiO_2/ZIF-8 photocatalysts compared to the values obtained with ZIF-8 (5 eV), depending on the mass fractions of TiO_2. The highest removal efficiency of imidacloprid was achieved with the hybrid photocatalysts containing 5 wt% TiO_2.

Keywords: imidacloprid; heterogeneous photocatalysis; metal-organic frameworks (MOFs); TiO_2; ZIF-8

check for updates

Citation: Bogdan, L.; Palčić, A.; Duplančić, M.; Leskovac, M.; Tomašić, V. Eco-Friendly Synthesis of TiO_2/ZIF-8 Composites: Characterization and Application for the Removal of Imidacloprid from Wastewater. *Processes* **2023**, *11*, 963. https://doi.org/10.3390/pr11030963

Academic Editor: Olivier Monfort

Received: 7 February 2023
Revised: 13 March 2023
Accepted: 15 March 2023
Published: 21 March 2023

1. Introduction

Due to the continuous increase in the concentration of organic pollutants, especially pesticides, in water ecosystems, there is a great need to find technology for efficient treatment of industrial and municipal wastewater. Concerns are particularly growing due to the presence of the widely used insecticide, imidacloprid, and neonicotinoids in general, in unintentionally treated areas in the form of dust generated by the operation of seed sowing machines, thereby affecting non-target beneficial insects [1,2]. Also, as it is soluble in water, imidacloprid has been observed in lakes and streams which presents a danger for various types of aquatic organisms [2–5]. Numerous studies have been conducted with the aim of studying the consequences of the use of imidacloprid on various species of bees and ladybugs. The studies showed an increase in mortality, damage to nervous system tissues, vision, and smell, as well as slowed growth and development of these insects. Moreover, drastic changes in their reproductive behavior were reported [6–8]. In addition, the systemic nature of imidacloprid enables the distribution of its metabolites within the plant, and its presence was detected in the nectar and pollen of some plants [2,9–14].

Over the past ten years metal-organic frameworks (MOFs) have received considerable attention as a research hotspot in both adsorption and photocatalysis [15–19]. It is worth highlighting the great chemical and functional adaptability of MOFs, which results from the use of different organic ligands, metals, and metal clusters, as well as different preparation methods and crystallization conditions. Various procedures for the synthesis of MOFs

are described in the literature (e.g., hydrothermal, solvothermal, mechanical, microwave, electrochemical, diffusion, ion thermal syntheses, etc.) [20,21]. The application of MOFs in the photocatalytic decomposition of organic pollutants and NO_x, antibacterial agents, solar fuels and for obtaining photoelectrochemical (PEC) energy further emphasizes the impressive potential of such materials [19,22–29]. Significant advances have also been made in the field of zeolites and advanced materials with a large specific surface area and uniform structure, which opens new possibilities for the preparation of composite photocatalysts and further improvement of the photocatalytic activity of existing photocatalysts whose constituent part is titanium dioxide [29–32]. The zeolitic imidazolate framework-8 (ZIF-8 or Zn (II)-imidazolate) consists of zinc (Zn) as a metal center and 2-methylimidazole (2-MIM) as organic linker. With Zn–N bond, ZIF-8 is one of the best known examples of stable framework structures in aqueous solutions [33,34]; it possesses higher chemical and thermal stability compared to other MOFs [35,36] and, in addition, its unique property is its superior adsorption capacity [37]. According to the opinion of some authors, the combination of ZIF-8 with appropriate semiconductor material reduces the recombination rate of charge carriers and enhances photocatalytic activity [38,39], thus making it a favorable candidate for utilization in photocatalytic processes.

Photocatalysis using titanium dioxide is a well-established method of decomposition of organic pollutants, yet the required activation by UV radiation presents a severe disadvantage that limits its use [40–42]. The attention of researchers in the field of photocatalysis is particularly focused on the innovative design of photocatalysts with the aim of solving problems related to band gap energy, charge transfer, and inhibition of photocatalytic reaction by charge recombination. The photocatalytic activity of existing photocatalysts, especially TiO_2, can be improved with various strategies, such as using organic and inorganic compounds as photosensitizers (dye sensitization), combining semiconductor materials of different energy levels, and doping/decoration with metals or nonmetals to inhibit the recombination rate and thus increase the quantum yield [43–46]. In the scope of extensive research in this area, various methods of doping titanium dioxide with nonmetals [47–49] or other photoactive metals [50–54] have been developed, as well as other TiO_2 modification procedures aimed at reducing the band gap as well as the rate of charged carrier recombination either by irradiating the surface with UV light [55] or by influencing the charge of the surface [56–62]. An expanding strategy of enhancing photoactivity is synthesizing composite materials by combining existing photocatalytic materials, such as TiO_2, with zeolites and mesoporous materials, as well as MOFs, thus taking advantage of the complementary benefits of different materials [63].

This study provides a simple and effective strategy for the rational design and fabrication of MOF-derived samples using an unconventional synthesis route as well as an environmentally friendly method of mechanochemical synthesis for the preparation of composite or hybrid materials that can be used for the low-cost and effective removal of a neonicotinoid insecticide (imidacloprid) from wastewater, combining the advantages of adsorption and photocatalysis utilizing TiO_2–the best known semiconductor photocatalyst so far–and ZIF-8, a representative of crystalline metal-organic framework materials, i.e., a relatively new and still insufficiently studied group of porous materials with extremely large application possibilities in various fields [64–69]. Photocatalysts based on MOFs can be considered third-generation photocatalysts [70]. However, the majority of photocatalytic degradation studies using MOFs are focused on the photodegradation of organic dyes [71]. To the best of our knowledge, this is the first report utilizing mechanochemically synthesized ZIF-8 and the hybrid TiO_2/ZIF-8 materials as possible photocatalytically active substances for pesticide removal.

2. Materials and Methods

2.1. Photocatalyst Synthesis

The synthesis of the photocatalyst was carried out in two stages. In the first stage, the metal-organic framework material ZIF-8 was synthesized mechanochemically, and in the second stage, hydrothermal synthesis was used to prepare the hybrid TiO_2/ZIF-8.

The ZIF-8 material was synthesized using the procedure proposed by Martinez et al. [64]. The mechanochemical synthesis lasted 55 min and was carried out in two steps. In the first part, 2-methylimidazole (Sigma Aldrich, St. Louis, MO, USA, 99%) and zinc oxide (Ventron, Mumbai, India, 99.9%) were added in two polymethylmethacrylate grinding jars in a mass ratio of 2:1. Two grinding balls made of zirconium dioxide with a diameter of 7 mm were added to the containers. The jars were closed, secured against the powder leakage, and placed in the Retsch MM 400 ball mill, Germany. The first phase of grinding was carried out for 10 min at a milling frequency of 30 Hz. After 10 min, the mill was stopped to add a few drops of ethanol (Gram Mol, Zagreb, Croatia, abs.) and several crystals of ammonium nitrate (TTT, Novaki, Croatia, p.a.) to the homogenized mixture of reactants. After this, the grinding vessels were again secured against powder leakage, the second stage of the mechanochemical synthesis lasted for 45 min at a grinding frequency of 30 Hz. At the end of the synthesis, the resultant powder was recovered from the milling jar ready for the characterization of the product.

Hydrothermal synthesis was used to prepare a TiO_2/ZIF-8 photocatalyst by employing autoclave-in-autoclave synthesis approach [69]. The ZIF-8 prepared by mechanochemical treatment was mixed in ethanol with titanium tetraisopropoxide (Acros, Geel, Belgium, 98%) at 300 rpm overnight. The prepared mixture was transferred to a 50 mL autoclave Teflon liner. Distilled water (6 mL) was placed in a 250 mL Teflon-lined steel autoclave and a 50 mL liner and the reaction mixture placed inside. Hydrothermal synthesis of the composite TiO_2/ZIF-8 photocatalyst was carried out overnight at 150 °C. Three composite photocatalysts with different mass fractions of titanium dioxide were synthesized, e.g., CAT-1 (5% TiO_2), CAT-2 (95% TiO_2) and CAT-3 (50% TiO_2). The system was cooled to room temperature and the product was washed with distilled water to neutral pH, which was followed by indicator paper. The resulting powdery product was dried in an oven at 65 °C.

2.2. Characterization of Photocatalysts

The crystallinity of ZIF-8 and synthesized dry powder catalysts was determined by X-ray diffraction (XRD) on Malvern PANalytical X'Pert Pro Multipurpose Powder Diffractometer, UK, under CuKα radiation (λ = 1.54 Å) at 40 kV and 8 mA. The infrared (IR) spectra was determined using the Frontier^{TM} FT-IR Spectrometer within the wavenumber 400 cm^{-1} and 4000 cm^{-1}. The band gap for mechanochemically synthesized ZIF-8 and hybrid catalysts was determined by using Tauc's method from the Kubelka-Munk function obtained by the Evolution^{TM} 350 Uv-Vis Spectrometer, Thermo Fisher, with a scan speed of 600 nm min^{-1}. The temperature stability of the samples was determined by thermogravimetric and calorimetric analysis (TGA-DSC). The TGA curves were determined by heating ~10 mg of the sample from 25 to 900 °C with a heating speed of 10 °C min^{-1} using TA Instruments Q500, USA, while the DSC curves were obtained on the Mettler Toledo DSC 823e by using two heating cycles, first from 25 to 105 °C and second from 25 to 250 °C (10 °C min^{-1}). The morphology and particle size of the powders were examined by a Tescan Vega 3 Easyprobe, Czech Republic, scanning electron microscope (SEM). The samples were steamed with gold and palladium. The particle size was also determined using laser diffraction on Mastersizer 2000, Malvern, UK, with particle refractive index (RI) 2.741 and dispersant RI 1.330.

2.3. Adsorption and Photocatalytic Experiments

The photocatalytic removal of imidacloprid (Sharda Cropchem Limited, Mumbai, India) was carried out in a suspension reactor using an aqueous solution of imidacloprid with

an initial concentration of 10 mg L^{-1}, a total reaction volume of 80 mL, and a photocatalyst mass of 80 mg at a constant mixing speed of 250 rpm. The irradiation source of the UV-A radiation was the Pen-Ray lamp, Upland, CA model 90-0019-01 with λ_{max} = 365 nm.

At the beginning and the end of the reaction, the following parameters were determined: pH value using a pH meter, and dissolved oxygen concentration measured with an oximeter. The initial pH value of the imidacloprid solution was ~5.3, and the desired pH value of 6.5 was achieved using a 0.01 M sodium hydroxide (VWR International, Leuven, Belgium) solution. The solution was mixed with a magnetic stirrer at room temperature at a speed of 250 rpm.

The photocatalytic removal of imidacloprid was carried out in a total period of 240 min. Before the photocatalytic process began, the reaction mixture was stirred for 30 min in the absence of light radiation to allow the adsorption equilibrium of imidacloprid molecules on the surface of the catalyst particles. After that, the lamp was inserted into the middle of the suspension reactor using a quartz tube. The photocatalytic reaction was monitored by taking aliquots of the reaction mixture (~0.5 mL) at certain time intervals (15, 30 and 60 min) and measuring the change in imidacloprid concentration using high performance liquid chromatography (HPLC) instrument (Shimadzu, Japan) equipped with a UV-Vis detector (254 nm). Separation and quantification were performed on an Agilent Zorbax C18 column (250 × 4.6 mm; 5 m, Santa Clara, CA, USA in gradient elution mode using two mobile phases of water and acetonitrile containing 0.3 v% formic acid at a flow rate of 1.0 cm^3 min^{-1}. In the initial period of the reaction, when the largest concentration changes were expected, measurements were performed every 15 min, then every 30 min and, after the 120th min of the reaction, every 60 min. Aliquots of the reaction mixture were filtered on a polyvinyl difluoride (PVDF) syringe microfilter (0.22 µm) and stored in ampoules for HPLC analysis. The change in the imidacloprid conversion and the evolution of the peak area of the photocatalytic transformation products detected by the LC-QToF-MS technique as a function of irradiation time for degradation over modified TiO_2 has been reported in previous work [55]. Since the photoactivity of pure ZIF-8 was not observed in the current study, we assume that a similar reaction mechanism can be attributed to the composites, as for TiO_2.

As mentioned, preliminary measurements included testing the equilibrium adsorption of the model component on the surface of the photocatalyst particles in an identical experimental system. The adsorption test was conducted in the absence of light i.e., with the photoreactor covered with aluminum foil.

3. Results and Discussion

The XRD patterns of the prepared hybrid samples were compared with the patterns of the mechanochemically synthesized ZIF-8 and commercial TiO_2 P25 obtained on the same device (Figure 1). It was found that the pattern of ZIF-8 is consistent with the literature data, with characteristic peaks at 2θ = 7.44°; 10.46°; 12.78°; 14.9°; 16.5° and 18° [64–69,72–75]. The newly formed hybrid composite catalysts CAT-1 and CAT-3 show a dominant ZIF-8 structure with characteristic peaks at 7.44°, 10.46° and 12.78°. The intense peak at 7.44° indicates that it is a highly crystalline form of ZIF-8 and the resulting composite. Indications of the peaks corresponding to the structure of TiO_2, specifically anatase in the structure of CAT-1 and CAT-2 composites, are also visible.

The synthesized CAT-2 catalyst largely coincides with the structure of TiO_2, more precisely with the structure of anatase with characteristic peaks at 25.28°, 37.93° and 48.34°. Such results were expected considering that the said hybrid predominantly contained TiO_2 (95%).

In Figure 2 the IR spectra of the synthesized composite photocatalysts with mechanochemically synthesized ZIF-8 is presented. In the "fingerprint" area (inset), the bands of CAT-1, CAT-3 and CAT-2 represent an overlap of ZIF-8 and TiO_2 bands depending on the corresponding proportion of each material in the samples. The small peaks at 3135 and 2929 cm^{-1} are associated with C-H stretching vibrations [76]. The absorption peaks between 1300 and

1500 cm^{-1} can be assigned to the entire ring stretching [77,78]. The peaks at 1147 and 995 cm^{-1} can be attributed to a C-N stretch mode [77,79], whereas the characteristic peaks at 760 cm^{-1} and 700 cm^{-1} could be assigned to a C-H bending mode and the ring out-of-plane bending vibration of the 2-methylimidazole (2-MIM), respectively [77]. Linear vibrations of the TiO_2 molecule exhibit bands in the region between 700 cm^{-1} and 500 cm^{-1}, yet are difficult for detection by FT-IR spectroscopic analysis as can be seen in the respective spectra of CAT-2 (95% TiO_2) and TiO_2. In addition, as the content of TiO_2 in CAT-1 and CAT-3 rises, the transmittance value of the ZIF-8 bands in that region decreases and the bands become less resolved. The FT-IR spectrum for pure TiO_2, shown in Figure 2, is in good agreement with earlier reports [80–83].

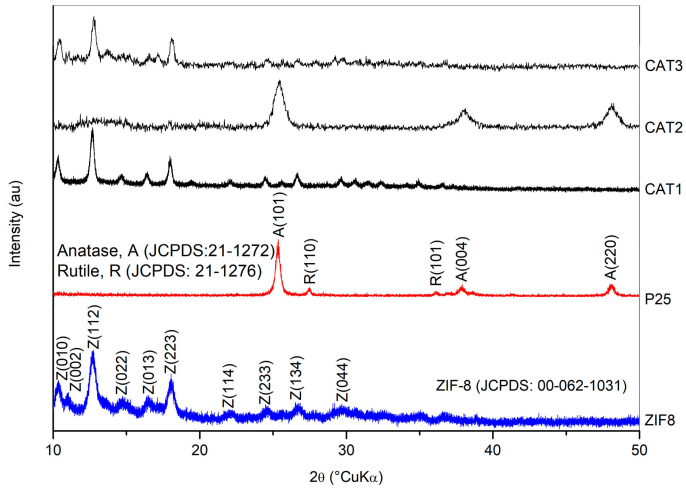

Figure 1. XRD patterns of the studied series of samples.

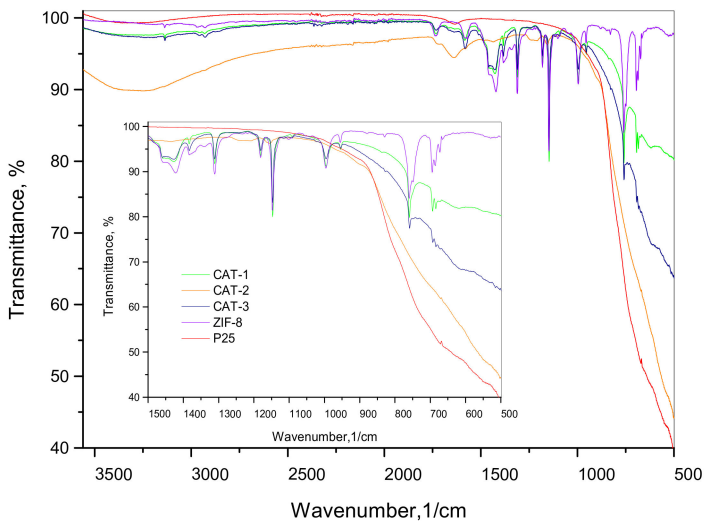

Figure 2. IR spectra of the studied series of samples.

Infrared spectroscopy was also used to gain insight into the adsorption of imidacloprid from a model solution on the surface of the composite catalysts. In the Figures S1 and S2, in Supplementary Materials, the IR spectra of ZIF-8, CAT-1, CAT-2 and CAT-3 are shown after application in the systems for testing adsorption and photocatalytic properties. Similarity of the spectra of used materials and the as-prepared materials indicates that during adsorption and during photocatalysis there is no change in the structure of the composite catalysts. The only difference is the presence of the band at 1310 cm^{-1} in the used samples so it can be assigned to imidacloprid. The highest intensity of this band for pure ZIF-8 sample suggests the largest amount of insecticide is adsorbed on the ZIF-8 sample.

The span of the band gap energy, E_g, is a very important parameter that is considered when examining the applicability of a photocatalyst in photocatalytic processes regarding wavelength range. Herein, the value of the energy gap was estimated using Tauc's method. It should be stressed that ZIF-8 is not a photocatalytically active substance. Mechanochemically synthesized ZIF-8 shows an energy gap value of 5.0 eV (Figure 3, inset). During the hydrothermal synthesis, a layer of titanium dioxide was applied to the surface of ZIF-8, which led to a reduction of the band gap energy of the resulting composites. It can be noted that the size of the band gap depends on the mass fraction of the photocatalytically active component, i.e., TiO_2. The addition of 5% titanium dioxide to the surface of ZIF-8 results in a reduction of the band gap from 5.0 eV to 3.6 eV, with 50% TiO_2 to 3.5 eV, and with 95% TiO_2 to 3.1 eV.

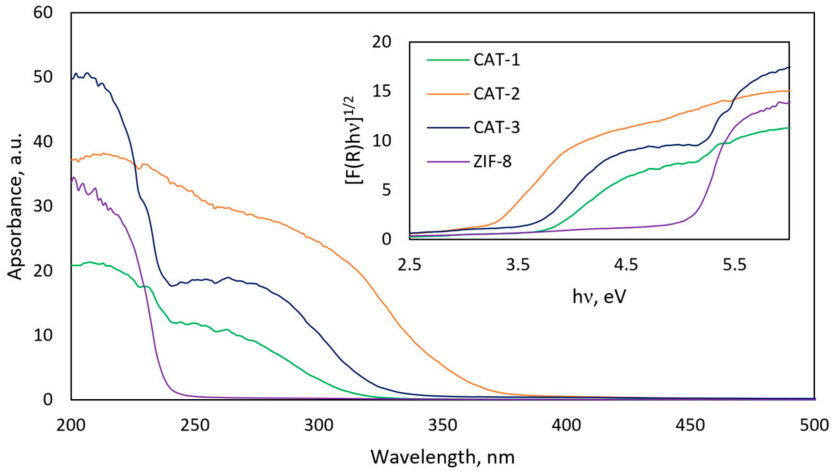

Figure 3. UV-Vis diffuse reflectance spectra and the Kubelka–Munk function of the studied samples (inset).

Thermogravimetric analysis (TG/TGA) and scanning calorimetric analysis (DSC) were performed to determine the thermal stability of the prepared samples. Thermogravimetric analysis (Figure S3A–H, Supplementary Materials) of all samples was carried out using TA Q500 in a stream of air and a stream of nitrogen, and the samples were heated from room temperature (~25 °C) to 900 °C.

Thermogravimetric analysis showed that both ZIF-8 and the hybrid catalysts are thermally stable and applicable in a wide range of temperatures up to 400 °C. Due to the high thermal stability of the inorganic components of the analyzed samples, it is assumed that water and smaller organic molecules remaining after the synthesis were removed in the early stages of the analysis, followed by the decomposition of ZIF-8 and 2-methylimidazole.

Next, a differential scanning calorimetry (DSC) analysis of the samples was carried out with two heating cycles (10 °C /min), the first from room temperature to 105 °C to remove excess water and organic matter remaining from the synthesis, and the second from room temperature to 250 °C. As can be seen in Figure S4 in Supplementary Materials, the DSC curves of all samples contain peaks that indicate an endothermic process, i.e., heat absorption. As it is an endothermic process, the area under the peak corresponds to the change in the latent heat of melting (ΔH_m) and is proportional to the amount of crystalline matter in the sample. Given that the expected dependence of the increase in crystallinity of the sample and the melting temperature depending on the mass fraction of TiO_2 was not observed, it is assumed that the crystallinity of the sample depends on the quality of the mechanochemically synthesized ZIF-8. Some researchers suggest that ZIF-8 recrystallizes in water which can cause the results to differ [74,75].

The morphology and size of the particles were examined by SEM and laser light diffraction. In Figure 4 the morphology of the samples obtained by SEM is shown. Particles of ZIF-8 and composite ZIF-8/TiO_2 photocatalysts form agglomerates of different sizes,

and it can be observed that larger agglomerates are formed in systems with more TiO_2 (CAT-2 and CAT-3). Meanwhile, CAT-1 and ZIF-8 form agglomerates of smaller sizes with characteristic dimensions up to approximately 20 µm; CAT-3 particles form agglomerates of 20–50 µm, while the dimensions of agglomerates in CAT-2 are greater than 50 µm.

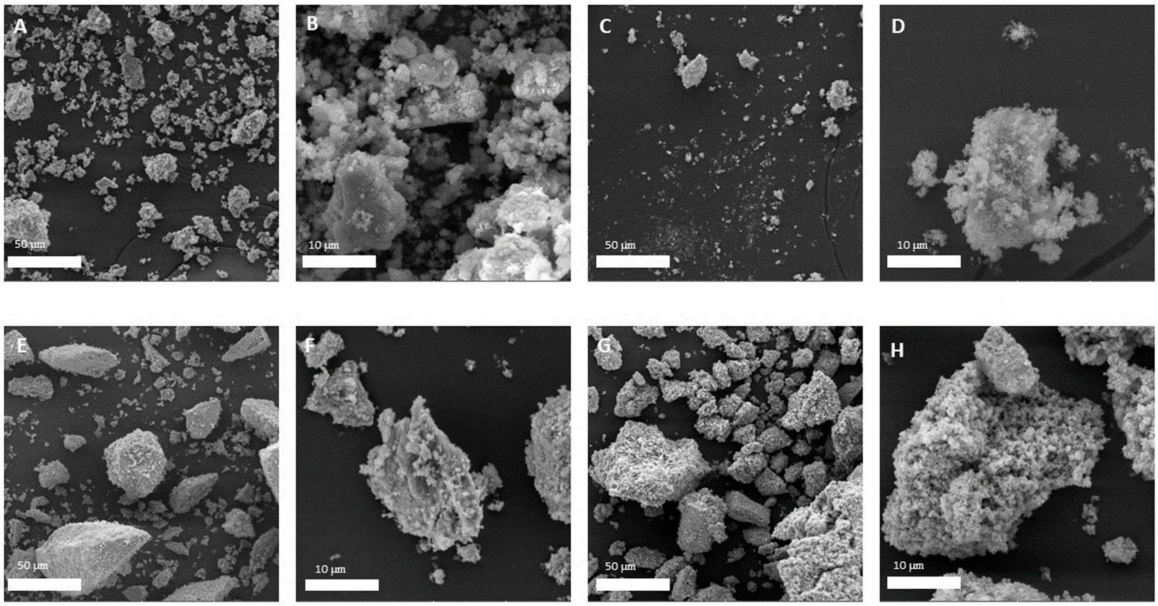

Figure 4. SEM images of the samples in 1kx (**A**,**C**,**E**,**G**) and 5kx (**B**,**D**,**F**,**H**) magnification for ZIF-8 (**A**,**B**), CAT-1 (**C**,**D**), CAT-2 (**E**,**F**) and CAT-3 (**G**,**H**).

The number-based particle size distribution is given in Figure 5. As the proportion of titanium dioxide in the photocatalyst gets higher, the particle size is shifted towards lower values and the width of the particle size distribution decreases. The largest proportion of particles in the ZIF-8 sample was observed between 0.357 µm and 0.485 µm, in CAT-1: 0.416–0.564 µm, in CAT-2: 0.278–0.377 µm, and in CAT-3: 0.285–0.377 µm. It can be observed that larger agglomerates are found in the samples containing particles of smaller sizes.

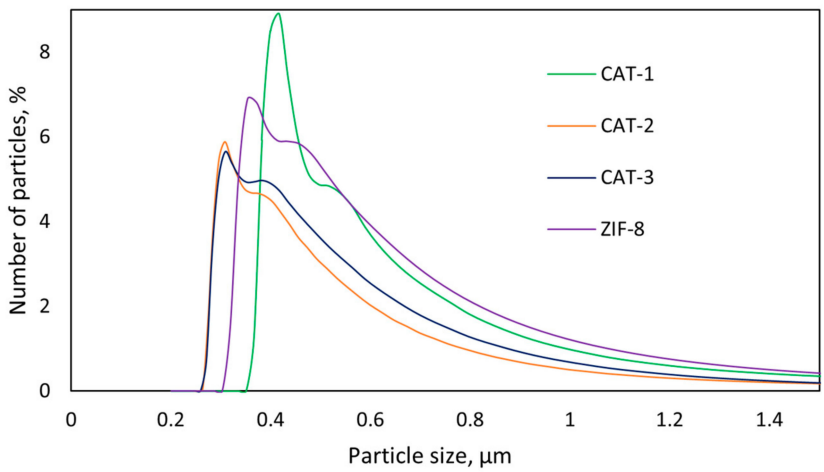

Figure 5. Particle size distribution of the prepared samples.

After the characterization of the samples, their adsorption and photocatalytic properties were tested in the system for the removal of the neonicotinoid insecticide, imidacloprid. Adsorption properties were tested in a suspension reactor in the absence of light, while

photocatalytic properties were tested in an identically prepared suspension reactor, with a centrally located Pen-Ray lamp as a source of UVA radiation. The ZIF-8 sample proved to be an extremely good adsorbent. After 120 min of conducting the experiment, it adsorbed 65% of the model component, and equilibrium adsorption of imidacloprid was achieved after approximately 30 min (Figure 6). On the other hand, the synthesized hybrid photocatalysts showed poor adsorption properties. In 120 min of conducting the experiment, only 1–3% of the model component was adsorbed. A possible reason for the reduced adsorption efficiency is the surface layer of titanium dioxide that blocks the active centers of ZIF-8 as well as the particle agglomeration.

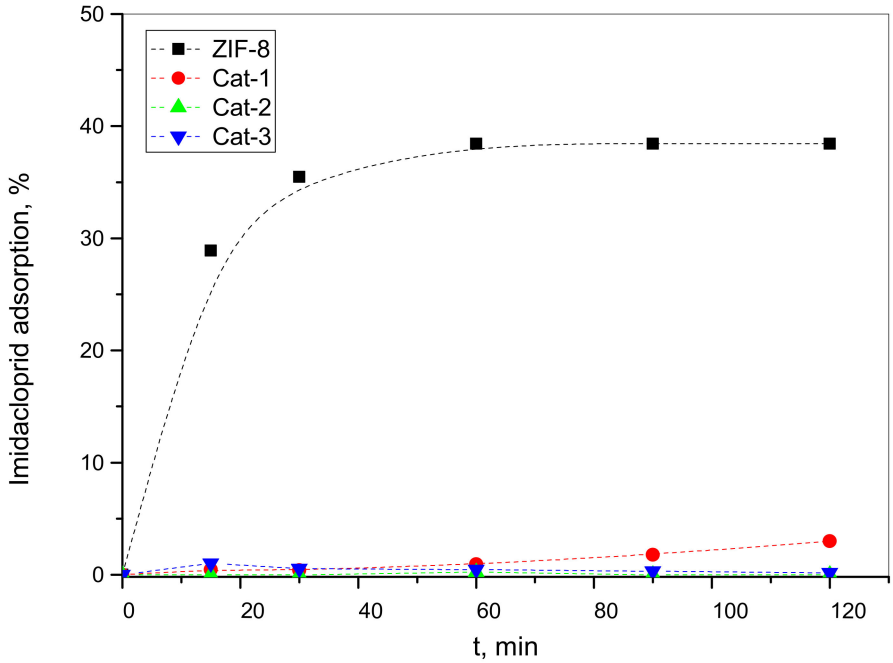

Figure 6. Adsorption of imidacloprid on mechanochemically synthesized ZIF-8 and on hybrid TiO_2/ZIF-8 samples.

Figure 6 illustrates the imidacloprid adsorption over mechanochemically synthesized ZIF-8 and hybrid TiO_2/ZIF-8 samples. The results obtained show that the adsorption capacity of ZIF-8 at an initial imidacloprid concentration of 1 g L^{-1} is 0.3842 mg g^{-1}, while the adsorption capacities of the composite samples are compatible with the TiO_2 content in the samples, i.e., the sample containing 5% TiO_2 (CAT-1) showed the highest adsorption capacity of 0.030 mg g^{-1}, followed by CAT-3 (50% TiO_2) with 0.0016 mg g^{-1}, while CAT-2, which contained 95% TiO_2, showed very low adsorption capacity. The results obtained are consistent with our expectations (e.g., the pure ZIF-8 exhibits the highest adsorption capacity) and as the TiO_2 weight fraction increased, the adsorption capacity of the hybrid samples decreased, which can be attributed to the low specific surface area of TiO_2.

Table S1 in Supplementary Materials gives an overview of the adsorption capacities of some MOF composites found in the literature and a comparison with the results obtained in this study [76,84–88].

After establishing the adsorption equilibrium, the reaction mixture was irradiated with a Pen-Ray lamp working at 365 nm. Figure 7 illustrates the changes of the normalized imidacloprid concentrations (C_A/C_{A0}) with irradiation time and testing the obtained results on the assumed model. The kinetic analysis was performed for a conventional batch reactor (closed system), assuming a pseudo-first-order kinetic model of reaction and root mean square deviations (RSMD) used as a correlation criterion between the experimental and theoretical data predicted by the proposed kinetic model. The estimated values of the pseudo-first-order rate constant (k_A) based on the experimental results using the method of

non-linear optimization and the RSMD are presented in Table 1. From the values of RMSD, it can be concluded that a good agreement of the experimental results with the values obtained to the assumed model has been achieved. The reaction rate constants, derived from the first-order kinetic curves (Figure 7) for the photodegradation of imidacloprid from the highest to the lowest, are given in the order of CAT-1 (9.129×10^{-4} min^{-1}), CAT-2 (7.790×10^{-4} min^{-1}) and CAT-3 (3.371×10^{-4} min^{-1}) catalysts.

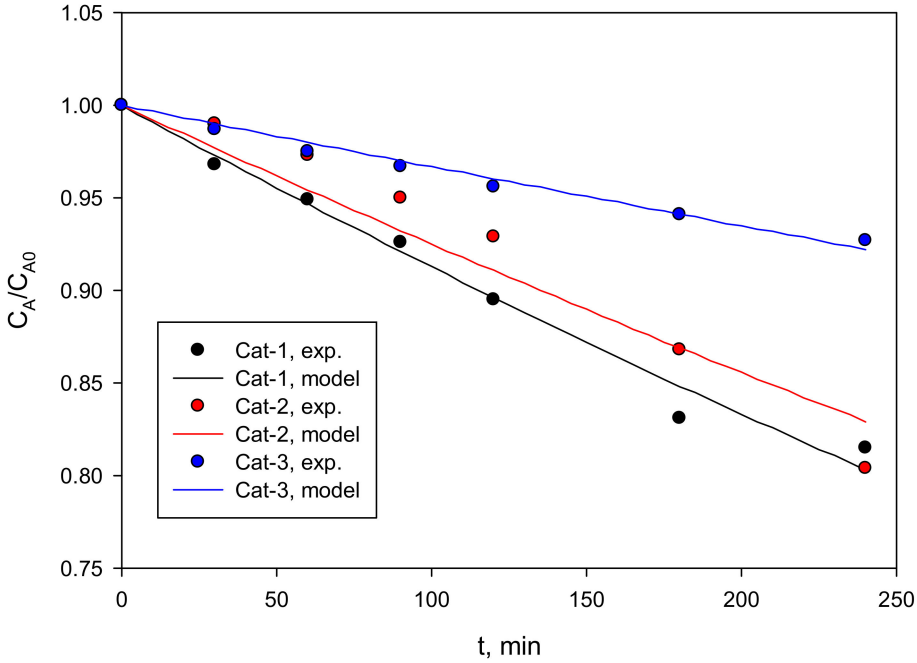

Figure 7. Pseudo-first-order kinetic curves of the imidacloprid photodegradation.

Table 1. Estimated values of the reaction rate constant (k_A) and the corresponding root mean square deviations (RMSD) for the kinetic model of pseudo-first-order.

Sample	k_A ($\times 10^4$), min^{-1}	RMSD $\times 10^3$
CAT-1	9.129	3.144
CAT-2	7.790	6.092
CAT-3	3.371	1.309

It is difficult to compare the kinetic results obtained with those in the literature due to either the lack of reported information or due to the different reaction conditions and photocatalysts applied. Examples dealing with photocatalytic degradation of imidacloprid or some other neonicotinoids via MOF-based composites are scarce and mostly refer to a different type of potential photocatalysts and various reaction conditions [89–91].

Figure 8 shows changes in pH and dissolved oxygen concentration during the photocatalytic process. The decrease in pH can be attributed to the formation of mineral salts during photocatalysis. During the photocatalytic removal of imidacloprid there is a decrease in the concentration of dissolved oxygen, which is in line with expectations. It is well known that the presence of oxygen reduces the recombination of charge carriers, i.e., oxygen as an electron acceptor with electrons of the conduction band (CB) can lead to the formation of superoxide anion radicals (O^{2-}), which play an extremely important role in the photodegradation mechanism of neonicotinoids.

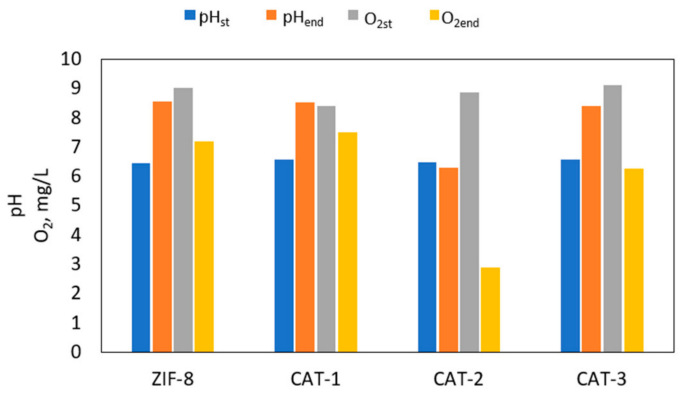

Figure 8. Changes in pH and dissolved oxygen concentration after photocatalytic tests (240 min).

Surprisingly, during the photocatalytic process there was an increase in the value of total organic carbon (not shown here). A possible explanation is that some of the organic molecules remained confined in the ZIF-8 samples during synthesis, which blocks the access of imidacloprid molecules to the catalytically active centers. A potential solution is the drying of hybrid photocatalysts during their preparation at slightly higher temperatures compared to the conditions used in this work (65 °C), especially since the thermal analysis showed a high thermal stability of the prepared samples. Nevertheless, it is observed that when ZIF-8 and the hybrid ZIF-8/TiO_2 are applied, the imidacloprid concentration decreases significantly, which is reflected in the imidacloprid removal efficiencies ranging from 8.4% to 55.1% (Figure 9).

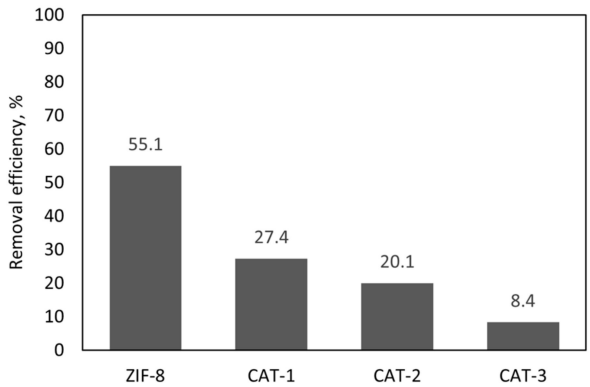

Figure 9. Comparison of the imidacloprid removal efficiency on different samples.

For the reusability experiments (Figure 10), the most active photocatalyst (CAT-1) was recovered by centrifugation at 600 rpm for 5 min, and the supernatant discarded. The photocatalyst was then dried at 65 °C for 6 h. The recovered powder was then poured into a fresh solution and used under the same conditions as in the previous photocatalytic experiments. After four cycles of measurement, the removal efficiency of imidacloprid slightly decreased with each cycle after 240 min of irradiation, which can be attributed to a slight loss of material during recycling, i.e., transferring from the centrifuge tube to the reaction vessel. The obtained results indicate the high stability of the photocatalyst under the specified operating conditions, which is particularly important for its practical application.

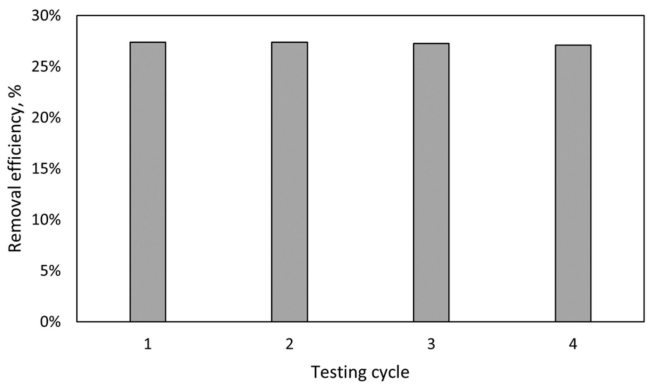

Figure 10. Reusability of CAT-1 for the photocatalytic removal of imidacloprid.

4. Conclusions

This work deals with the preparation, detailed characterization, and application of hybrid photocatalysts for the removal of imidacloprid as a representative of agricultural pollutants. Hybrid photocatalysts were prepared by an innovative method that combines the advantages of mechanochemical and hydrothermal synthesis. The aim of the syntheses was to combine TiO_2 as a proven photocatalytically active component and ZIF-8 as representative of zeolitic imidazolate frameworks that possess unique structural, textural and physico-chemical properties and, therefore, are promising materials for the preparation of the hybrid photocatalysts. Our intention was to improve the adsorption capacity and to reduce the band gap energies which, as expected, would result in a shift of the working area of the hybrid TiO_2/ZIF-8 photocatalyst towards the wavelengths of the visible region of solar radiation. A detailed characterization was carried out using different methods, such as XRD, infrared spectroscopy, UV/Vis spectroscopy, thermogravimetry, DSC analysis, SEM and the laser diffraction method.

The obtained results show that hybrid TiO_2/ZIF-8 materials with favorable adsorption properties and reduced band gap energies compared to ZIF-8 can be successfully prepared by using the method described in this study. Although the prepared hybrid photocatalysts showed only moderate and still insufficient activity, we believe that this work provides useful guidelines for the design and development of new hybrid photocatalysts with great potential for visible light application for environmental remediation.

Supplementary Materials: The following supporting information can be downloaded at: https://www.mdpi.com/article/10.3390/pr11030963/s1, Figure S1: IR spectra of the samples after imidacloprid adsorption, Figure S2: IR spectra of the samples after photocatalytic testing, Figure S3: TGA curves of the samples in nitrogen (A, C, E, G) and air (B, D, F, H) for mechanochemically synthesized ZIF-8 (A, B), CAT-1 (C, D), CAT-2 (E, F) and CAT-3 (G, H), Figure S4: DSC curves of the studied series of samples; Table S1: An overview of the adsorption capacities of MOF composites found in literature.

Author Contributions: Conceptualization, A.P., M.D. and V.T.; methodology, A.P. and M.D.; investigation, L.B. and M.D.; resources, A.P. and V.T.; data curation, L.B., A.P., M.D. and M.L.; writing-original draft preparation, L.B.; writing-review and editing, A.P. and V.T.; visualization, L.B. and M.D.; supervision, A.P. and V.T.; funding acquisition, A.P. and V.T. All authors have read and agreed to the published version of the manuscript.

Funding: The research was funded by the Croatian Science Foundation under the projects IN-PhotoCat (IP-2018-01-8669) and SMALLPORE (UIP-2019-04-4977).

Data Availability Statement: The data presented in this study are available upon reasonable request from the corresponding authors.

Conflicts of Interest: The authors declare no conflict of interest.

References

1. Jeschke, P.; Nauen, R.; Schindler, M.; Elbert, A. Overview of the status and global strategy for neonicotinoids. *J. Agric. Food Chem.* **2011**, *59*, 2897–2908. [CrossRef] [PubMed]
2. Wood, T.J.; Goulson, D. The environmental risks of neonicotinoid pesticides: A review of the evidence post 2013. *Environ. Sci. Pollut. Res.* **2017**, *24*, 17285–17325. [CrossRef] [PubMed]
3. Goulson, D. Review: An overview of the environmental risks posed by neonicotinoid insecticides. *J. Appl. Ecol.* **2013**, *50*, 977–987. [CrossRef]
4. Hladik, M.L.; Kolpin, D.W. First national-scale reconnaissance of neonicotinoid insecticides in streams across the USA. *Environ. Chem.* **2016**, *13*, 12–20. [CrossRef]
5. Morrissey, C.A.; Mineau, P.; Devries, J.H.; Sanchez-Bayo, F.; Liess, M.; Cavallaro, M.; Liber, K. Neonicotinoid contamination of global surface waters and associated risk to aquatic invertebrates: A review. *Environ. Int.* **2015**, *74*, 291–303. [CrossRef]
6. Calvo-Agudo, M.; González-Cabrera, J.; Picó, Y.; Calatayud-Vernich, P.; Urbaneja, A.; Dicke, M.; Tena, A. Neonicotinoids in excretion product of phloem-feeding insects kill beneficial insects. *Proc. Natl. Acad. Sci. USA* **2019**, *116*, 16817–16822. [CrossRef] [PubMed]
7. Crall, J.; Switzer, C.; Oppenheimer, R.; Ford Versypt, A.; Dey, B.; Brown, A.; Eyster, M.; Guérin, C.; Pierce, N.; Combes, S.; et al. Neonicotinoid exposure disrupts bumblebee nest behavior, social networks, and thermoregulation. *Science* **2018**, *362*, 683–686. [CrossRef]
8. Decourtye, A.; Lacassie, E.; Pham-Delègue, M.H. Learning performances of honeybees (*Apis mellifera* L.) are differentially affected by imidacloprid according to the season. *Pest Manag. Sci.* **2003**, *59*, 269–278. [CrossRef]
9. Seccia, S.; Fidente, P.; Barbini, D.A.; Morrica, P. Multiresidue determination of nicotinoid insecticide residues in drinking water by liquid chromatography with electrospray ionization mass spectrometry. *Anal. Chim. Acta* **2005**, *553*, 21–26. [CrossRef]
10. Klarich, K.L.; Pflug, N.C.; DeWald, E.M.; Hladik, M.L.; Kolpin, D.W.; Cwiertny, D.M.; LeFevre, G.H. Occurrence of neonicotinoid insecticides in finished drinking water and fate during drinking water treatment. *Environ. Sci. Technol.* **2017**, *4*, 168–173. [CrossRef]
11. Xie, W.; Han, C.; Qian, Y.; Ding, H.; Chen, X.; Xi, J. Determination of neonicotinoid pesticides residues in agricultural samples by solid-phase extraction combined with liquid chromatography–tandem mass spectrometry. *J. Chromatogr. A* **2011**, *1218*, 4426–4433. [CrossRef] [PubMed]
12. Seccia, S.; Fidente, P.; Montesano, D.; Morrica, P. Determination of neonicotinoid insecticides residues in bovine milk samples by solid-phase extraction clean-up and liquid chromatography with diode-array detection. *J. Chromatogr. A* **2008**, *1214*, 115–120. [CrossRef]
13. Mitchell, E.; Mulhauser, B.; Mulot, M.; Mutabazi, A.; Glauser, G.; Aebi, A. A worldwide survey of neonicotinoids in honey. *Science* **2017**, *358*, 109–111. [CrossRef] [PubMed]
14. Venieri, D.; Mantzavinos, D. Disinfection of waters/wastewaters by solar photocatalysis. In *Advances in Photocatalytic Disinfection*; An, T., Zhao, H., Wong, P., Eds.; Springer: Berlin/Heidelberg, Germany, 2017; pp. 177–198.
15. Kuppler, R.; Timmons, D.; Fang, Q.; Li, J.; Makal, T.; Young, M.; Yuan, D.; Zhao, D.; Zhuang, W.; Zhou, H. Potential applications of metal-organic frameworks. *Coord. Chem. Rev.* **2009**, *253*, 3042–3066. [CrossRef]
16. Mouchaham, G.; Wang, S.; Serre, C. The stability of metal-organic frameworks. In *Metal-Organic Frameworks: Applications in Separations and Catalysis*, 1st ed.; García, H., Navalón, S., Eds.; Wiley-VCH Verlag GmbH & Co. KGaA: Weinheim, Germany, 2018; pp. 1–28.
17. Alshammari, A.; Jiang, Z.; Cordova, K.E. Metal-organic frameworks as emerging photocatalysts. In *Semiconductor Photocatalysis—Materials, Mechanisms and Applications*; Cao, W., Ed.; IntechOpen: London, UK, 2016; pp. 301–341.
18. Li, J.R.; Sculley, J.; Zhou, H.C. Metal–organic frameworks for separations. *Chem. Rev.* **2012**, *112*, 869–932. [CrossRef]
19. Mallick, A.; Schön, E.M.; Panda, T.; Sreenivas, K.; Díaz, D.D.; Banerjee, R. Fine-tuning the balance between crystallization and gelation and enhancement of CO_2 uptake on functionalized calcium based MOFs and metallogels. *J. Mater. Chem.* **2012**, *22*, 14951–14963. [CrossRef]
20. Tchinsa, A.; Hossain, M.F.; Wang, T.; Zhou, Y. Removal of organic pollutants from aqueous solutions using metal organic frameworks (MOFs)-based adsorbens; A review. *Chemosphere* **2021**, *284*, 131393. [CrossRef] [PubMed]
21. Binling, C.; Zhuxian, Y.; Yanqiu, Z.; Yongde, X. Zeolitic imidazolate framework materials: Recent progress in synthesis and application. *J. Mater. Chem. A* **2014**, *2*, 16811–16831. [CrossRef]
22. Liu, C.; Li, F.; Ma, L.P.; Cheng, H.M. Advanced materials for energy storage. *Adv. Mater.* **2010**, *22*, 28–62. [CrossRef]
23. Li, J.R.; Kuppler, R.J.; Zhou, H.C. Selective gas adsorption and separation in metal–organic frameworks. *Chem. Soc. Rev.* **2009**, *38*, 1477–1504. [CrossRef]
24. Zacher, D.; Shekhah, O.; Wöll, C.; Fischer, R.A. Thin films of metal–organic frameworks. *Chem. Soc. Rev.* **2009**, *38*, 1418–1429. [CrossRef] [PubMed]
25. Bradshaw, D.; Garai, A.; Huo, J. Metal–organic framework growth at functional interfaces: Thin films and composites for diverse applications. *Chem. Soc. Rev.* **2012**, *41*, 2344–2381. [CrossRef]
26. Yu, J.; Cui, Y.; Xu, H.; Yang, Y.; Wang, Z.; Chen, B.; Qian, G. Confinement of pyridinium hemicyanine dye within an anionic metal-organic framework for two-photon-pumped lasing. *Nat. Commun.* **2013**, *4*, 2719. [CrossRef] [PubMed]

27. Zhang, S.; Du, D.; Tan, K.; Qin, J.; Dong, H.; Li, S.; He, W.; Lan, Y.; Shem, P.; Su, Z. Self-Assembly versus stepwise synthesis: Heterometal-organic frameworks based on metalloligands with tunable luminescence properties. *Chem. Eur. J.* **2013**, *19*, 11279–11286. [CrossRef]
28. Lee, J.; Farha, O.K.; Roberts, J.; Scheidt, K.A.; Nguyen, S.T.; Hupp, J.T. Metal–organic framework materials as catalysts. *Chem. Soc. Rev.* **2009**, *38*, 1450–1459. [CrossRef] [PubMed]
29. Navarro Amador, R.; Carboni, M.; Meyer, D. Photosensitive titanium and zirconium metal-organic frameworks: Current research and future possibilities. *Mater. Lett.* **2016**, *166*, 327–338. [CrossRef]
30. Horiuchi, Y.; Toyao, T.; Takeuchi, M.; Matsuoka, M.; Anpo, M. Recent advances in visible-light-responsive photocatalysts for hydrogen production and solar energy conversion—From semiconducting TiO_2 to MOF/PCP photocatalysts. *Phys. Chem. Chem. Phys.* **2013**, *15*, 13243–13253. [CrossRef]
31. Wang, C.; Li, J.; Lv, X.; Zhang, Y.; Guo, G. Photocatalytic organic pollutants degradation in metal–organic frameworks. *Energy Environ. Sci.* **2014**, *7*, 2831–2867. [CrossRef]
32. Konnerth, H.; Matsagar, B.M.; Chen, S.S.; Prechtl, M.H.G.; Shieh, F.K.; Wu, K.C.W. Metal-organic framework (MOF)-derived catalysts for fine chemical production. *Coord. Chem. Rev.* **2020**, *416*, 213319. [CrossRef]
33. Han, S.S.; Choi, S.H.; Van Duin, A. C:T. Molecular dynamics simulations of stability of metal-organic frameworks against H_2O using the ReaxFF reactive force field. *Chem. Commun.* **2010**, *46*, 5713–5715. [CrossRef]
34. Fatta- Kassinos, D.; Meric, S.; Nikolaou, A. Pharmaceutical residues in environmental waters and wastewater: Current state of knowledge and future research. *Anal. Bioanal. Chem.* **2011**, *399*, 251–275. [CrossRef]
35. Pouramini, Z.; Mousavi, S.M.; Babapoor, A.; Hashemi, S.A.; Lai, C.W.; Mazaheri, Y.; Chiang, W.H. Effect of metal atom in zeolitic imidazolate frameworks (ZIF-8 & 67) for removal of dyes and antibiotics from wastewater: A review. *Catalysts* **2023**, *13*, 155.
36. Abdollahi, B.; Najafidoust, A.; Asl, E.A.; Sillanpaa, M. Fabrication of ZIF-8 metal organic framework (MOFs) based CuO-ZnO photocatalyst with enhanced solar-light-driven property for degradation of organic dyes. *Arabian J. Chem.* **2021**, *14*, 103444. [CrossRef]
37. Tran, B.L.; Chin, H.Y.; Chang, B.K.; Chiang, A.S.T. Dye adsorption in ZIF-8: The importance of external surface area. *Microporous Mesoporous Mater.* **2019**, *277*, 149–153. [CrossRef]
38. Liu, Y.; Cheng, H.; Cheng, M.; Liu, Z.; Huang, D.; Zhang, G.; Shao, B.; Liangf, Q.; Luo, S.; Wu, T.; et al. The application of zeolitic imidazolate frameworks (ZIFs) and their derivates based materials for photocatalytic hydrogen evolution and pollutants treatment. *Chem. Eng. J.* **2021**, *417*, 127914. [CrossRef]
39. Tuncel, D.; Ökte, A.N. Improved adsorption capacity and photoactivity of ZnO-ZIF-8 nanocomposites. *Catal. Today* **2021**, *361*, 191–197. [CrossRef]
40. Farré, M.; Pérez, S.; Kantiani, L.; Barceló, D. Fate and toxicity of emerging pollutants, their metabolites and transformation products in the aquatic environment. *Trends Anal.Chem.* **2008**, *27*, 991–1007. [CrossRef]
41. Liu, L.; Bai, H.; Liu, J.; Sun, D.D. Multifunctional graphene oxide-TiO_2-Ag nanocomposites for high performance water disinfection and decontamination under solar irradiation. *J. Hazard. Mater.* **2013**, *261*, 214–223. [CrossRef]
42. Thind, S.S.; Wu, G.; Chen, A. Synthesis of mesoporous nitrogen–tungsten co-doped TiO_2 photocatalysts with high visible light activity. *Appl. Catal. B* **2012**, *111–112*, 38–45. [CrossRef]
43. Rehman, Z.U.; Bilal, M.; Hou, J.; Butt, F.K.; Ahmad, J.; Ali, S.; Hussain, A. Photocatalytic CO_2 reduction using TiO_2-based photocatalysts and TiO_2 z-scheme heterojunction composites: A review. *Molecules* **2022**, *27*, 2069. [CrossRef]
44. Chong, M.N.; Jin, B.; Chow, C.W.K.; Saint, C. Recent developments in photocatalytic water treatment technology: A review. *Water Res.* **2010**, *44*, 2997–3027. [CrossRef] [PubMed]
45. Ochiai, T.; Fujishima, A. Photocatalysis and water purification: From fundamentals to recent applications. In *Photocatalysis and Water Purification*; Pichat, P., Ed.; Wiley-VCH: Weinheim, Germany, 2013; pp. 361–373.
46. Fagan, R.; McCormack, D.E.; Dionysiou, D.D.; Pillai, S.C. A review of solar and visible light active TiO_2 photocatalysts for treating bacteria, cyanotoxins and contaminants of emerging concern. *Mat. Sci. Semicond. Process* **2016**, *42*, 2–14. [CrossRef]
47. Xu, J.; Wang, W.; Sun, S.; Wang, L. Enhancing visible-light-induced photocatalytic activity by coupling with wide-band-gap semiconductor: A case study on Bi_2WO_6/TiO_2. *Appl. Catal. B* **2012**, *111–112*, 126–132. [CrossRef]
48. Zhao, W.; Ma, W.; Chen, C.; Zhao, J.; Shuai, Z. Efficient degradation of toxic organic pollutants with Ni_2O_3/TiO_2-xB_x under visible irradiation. *J. Am. Chem. Soc.* **2004**, *126*, 4782–4783. [CrossRef]
49. Ma, J.; Xiong, Z.; Waite, D.T.; Ng, W.J.; Zhao, X.S. Enhanced inactivation of bacteria with silver-modified mesoporous TiO_2 under weak ultraviolet irradiation. *Microporous Mesoporous Mater.* **2011**, *144*, 97–104. [CrossRef]
50. Oros-Ruiz, S.; Zanella, R.; Prado, B. Photocatalytic degradation of trimethoprim by metallic nanoparticles supported on TiO_2-P25. *J. Hazard. Mater.* **2013**, *263*, 28–35. [CrossRef] [PubMed]
51. Fang, H.; Zhang, C.X.; Liu, L.; Zhao, Y.M.; Xu, H.J. Recyclable three-dimensional Ag nanoparticle-decorated TiO_2 nanorod arrays for surface-enhanced Raman scattering. *Biosens. Bioelectron.* **2015**, *64*, 434–441. [CrossRef]
52. Zhang, X.; Zhu, Y.; Yang, X.; Wang, S.; Shen, J.; Lin, B.; Li, C. Enhanced visible light photocatalytic activity of interlayer-isolated triplex Ag@SiO_2@TiO_2 core–shell nanoparticles. *Nanoscale* **2013**, *5*, 3359–3366. [CrossRef]
53. Pulido Melián, E.; González Díaz, O.; Doña Rodríguez, J.M.; Colon, G.; Navio, J.A.; Marcias, M.; Pérez Peña, J. Effect of deposition of silver on structural characteristics and photoactivity of TiO_2-based photocatalysts. *Appl. Catal. B* **2012**, *127*, 112–120. [CrossRef]

54. Liu, C.; Lei, Z.; Yang, Y.; Wang, H.; Zhang, Z. Improvement in settleability and dewaterability of waste activated sludge by solar photocatalytic treatment in Ag/TiO_2-coated glass tubular reactor. *Bioresour. Technol.* **2013**, *137*, 57–62. [CrossRef]
55. Babić, K.; Tomašić, V.; Gilja, V.; Le Cunff, J.; Gomzi, V.; Pintar, A.; Žerjav, G.; Kurajica, S.; Duplančić, M.; Zelić, I.E.; et al. Photocatalytic degradation of imidacloprid in the flat-plate photoreactor under UVA and simulated solar irradiance conditions—The influence of operating conditions, kinetics and degradation pathway. *J. Environ. Chem. Eng.* **2021**, *9*, 105611.
56. Vohra, M.S.; Lee, J.; Choi, W. Enhanced photocatalytic degradation of tetramethylammonium on silica-loaded titania. *J. Appl. Electrochem.* **2005**, *35*, 757–763. [CrossRef]
57. Fu, X.; Clark, L.A.; Yang, Q.; Anderson, M.A. Enhanced photocatalytic performance of titania-based binary metal oxides: TiO_2/SiO_2 and TiO_2/ZrO_2. *Environ. Sci. Technol.* **1996**, *30*, 647–653. [CrossRef]
58. Anderson, C.; Bard, A.J. Improved photocatalytic activity and characterization of mixed TiO_2/SiO_2 and TiO_2/Al_2O_3 materials. *J. Phys. Chem. B* **1997**, *101*, 2611–2616. [CrossRef]
59. Anderson, C.; Bard, A.J. An improved photocatalyst of TiO_2/SiO_2 prepared by a sol-gel synthesis. *J. Phys. Chem.* **1995**, *99*, 9882–9885. [CrossRef]
60. Chun, H.; Yizhong, W.; Hongxiao, T. Influence of adsorption on the photodegradation of various dyes using surface bond-conjugated TiO_2/SiO_2 photocatalyst. *Appl. Catal. B* **2001**, *35*, 95–105. [CrossRef]
61. Zhang, G.; Choi, W.; Kim, S.H.; Hong, S.B. Selective photocatalytic degradation of aquatic pollutants by titania encapsulated into FAU-type zeolites. *J. Hazard. Mater.* **2011**, *188*, 198–205. [CrossRef]
62. Artkla, S.; Kim, W.; Choi, W.; Wittayakun, J. Highly enhanced photocatalytic degradation of tetramethylammonium on the hybrid catalyst of titania and MCM-41 obtained from rice husk silica. *Appl. Catal. B* **2009**, *91*, 157–164. [CrossRef]
63. Dahl, M.; Liu, Y.; Yin, Y. Composite Titanium Dioxide Nanomaterials. *Chem. Rev.* **2014**, *114*, 9853–9889. [CrossRef]
64. Martinez, V.; Karadeniz, B.; Biliškov, N.; Lončarić, I.; Muratović, S.; Žilić, D.; Avdoshenko, S.; Roslova, M.; Popov, A.; Užarević, K. Tunable fulleretic sodalite MOFs: Highly efficient and controllable entrapment of C_{60} fullerene via mechanochemistry. *Chem. Mater.* **2020**, *32*, 10628–10640. [CrossRef]
65. Park, K.; Ni, Z.; Côté, A.; Choi, J.; Huang, R.; Uribe-Romo, F.; Chae, H.; O'Keeffe, M.; Yaghi, O. Exceptional chemical and thermal stability of zeolitic imidazolate frameworks. *Proc. Natl. Acad. Sci. USA* **2006**, *103*, 10186–10191. [CrossRef] [PubMed]
66. Pan, Y.; Liu, Y.; Zeng, G.; Zhao, L.; Lai, Z. Rapid synthesis of zeolitic imidazolate framework-8 (ZIF-8) nanocrystals in an aqueous system. *Chem. Comm.* **2011**, *47*, 2071–2073. [CrossRef] [PubMed]
67. Užarević, K.; Ferdelji, N.; Mrla, T.; Julien, P.; Friščić, T.; Halasz, I. Enthalpy vs. friction: Heat flow modelling of unexpected temperature profiles in mechanochemistry of metal–organic frameworks. *Chem. Sci.* **2018**, *9*, 2525–2532. [CrossRef] [PubMed]
68. Akimbekov, Z.; Katsenis, A.; Nagabhushana, G.; Ayoub, G.; Arhangelskis, M.; Morris, A.; Friščić, T.; Navrotsky, A. Experimental and theoretical evaluation of the stability of true MOF polymorphs explains their mechanochemical interconversions. *J. Am. Chem. Soc.* **2017**, *139*, 7952–7957. [CrossRef]
69. Li, R.; Li, W.; Jin, C.; He, Q.; Wang, Y. Fabrication of ZIF-8@TiO_2 micron composite via hydrothermal method with enhanced absorption and photocatalytic activities in tetracycline degradation. *J. Alloys Compd.* **2020**, *825*, 154008–154018. [CrossRef]
70. Hayati, P.; Mehrabadi, Z.; Karini, M.; Janczak, J.; Mohammadi, K.; Mahmoudi, G.; Dadi, F.; Fard, M.J.S.; Hasanzadeh, A.; Rostamnia, S. Photocatalytic activity of new nanostructures of an Ag(I) metal-organic framework (Ag-MOF) for efficient degradation of MCPA and 2,4-D herbicides under sunlight irradiation. *New J. Chem.* **2021**, *45*, 3408–3417. [CrossRef]
71. Naghdi, S.; Shahrestani, M.M.; Zendehbad, M.; Djahaniani, H.; Kazemian, H.; Eder, D. Recent advances in application of metal-organic frameworks (MOFs) as adsorbent and catalyst in removal of persistent organic pollutants (POPs). *J. Hazard. Mat.* **2023**, *442*, 130127. [CrossRef]
72. Wang, S.; Zhang, S. Study on the structure activity relationship of ZIF-8 synthesis and thermal stability. *J. Inorg. Organomet. Polym. Mater.* **2017**, *27*, 1317–1322. [CrossRef]
73. James, J.; Lin, Y. Kinetics of ZIF-8 thermal decomposition in inert, oxidizing, and reducing environments. *J. Phys. Chem. C* **2016**, *120*, 14015–14026. [CrossRef]
74. Zhang, H.; Zhao, M.; Lin, Y. Stability of ZIF-8 in water under ambient conditions. *Microporous Mesoporous Mater.* **2019**, *279*, 201–210. [CrossRef]
75. Zhang, H.; Zhao, M.; Yang, Y.; Lin, Y. Hydrolysis and condensation of ZIF-8 in water. *Microporous Mesoporous Mater.* **2019**, *288*, 109568. [CrossRef]
76. Li, T.; Lu, M.; Gao, Y.; Huang, X.; Liu, G.; Xu, D. Double layer MOFs M-ZIF-8@ZIF-67: The adsorption capacity and removal mechanism of fipronil and its metabolites from environmental water and cucumber samples. *J. Adv. Res.* **2020**, *24*, 159–166. [CrossRef]
77. Zhang, Y.; Jia, Y.; Li, M.; Hou, L. Influence of 2-methylimidazole/zinc nitrate hexahydrate molar ration on the synthesis of zeolitic imidazole framework-8 crystals at room temperature. *Sci. Rep.* **2018**, *8*, 9597. [CrossRef] [PubMed]
78. Hu, Y.; Kazemian, H.; Rohani, S.; Huang, Y.; Song, Y. In situ high pressure study of ZIF-8 by FTIR spectroscopy. *Chem. Commun.* **2011**, *47*, 12694–12696. [CrossRef]
79. Ordoñez, M.J.C.; Balkus, K.J.; Ferraris, J.P.; Musselman, I.H. Molecular sieving realized with ZIF-8/ Matrimid® mixed-matrix membranes. *J. Membr. Sci.* **2010**, *361*, 28–37. [CrossRef]
80. Al-Oubidy, E.A.; Kadhim, F.J. Photocatalytic activity of anatase titanium dioxide nanostructures prepared by reactive magnetron sputtering technique. *Opt. Quantum Electron.* **2019**, *51*, 23. [CrossRef]

81. Kadadevarmath, J.S. A simple approach on synthesis of TiO_2 nanoparticles and its application in dye sensitized solar cells. *J. Nano-Electron. Phys.* **2017**, *9*, 04005.
82. Zewde, B.; Pitliya, P.; Raghavan, D. The role of surface modified TiO_2 nanoparticles on the mechanical and thermal properties of CTBN toughened epoxy nanocomposite. *J. Mater. Sci.* **2016**, *51*, 9314–9329. [CrossRef]
83. Wang, G.; Xu, L.; Zhang, J.; Yin, T.; Deyan, H. Enhanced photocatalytic activity of TiO_2 powders (P25) via calcination treatment. *Int. J. Photoenergy* **2011**, *2012*, 265760.
84. Liu, G.; Li, L.; Huang, X.; Zheng, S.; Xu, X.; Liu, Z.; Zhang, Y.; Wang, J.; Lin, H.; Xu, D. Adsorption and removal of organophosphorus pesticides from environmental water and soil samples by using magnetic multi-walled carbon nanotubes@organic framework ZIF-8. *J. Mater. Sci.* **2018**, *53*, 10772–10783. [CrossRef]
85. Liu, G.; Li, L.; Xu, D.; Huang, X.; Xu, X.; Zheng, S.; Zhang, Y.; Lin, H. Metal–organic framework preparation using magnetic graphene oxide-β-cyclodextrin for neonicotinoid pesticide adsorption and removal. *Carbohydr. Polym.* **2017**, *175*, 584–591. [CrossRef] [PubMed]
86. Hasan, Z.; Jhung, S.H. Removal of hazardous organics from water using metal-organic frameworks (MOFs): Plausible mechanisms for selective adsorptions. *J. Hazard. Mater.* **2015**, *283*, 329–339. [CrossRef] [PubMed]
87. Rojas, S.; Horcajada, P. Metal-organic frameworks for the removal of emerging organic contaminants in water. *Chem. Rev.* **2010**, *120*, 8378–8415. [CrossRef] [PubMed]
88. Mahmoud, L.A.M.; dos Reis, R.A.; Chen, X.; Ting, V.P.; Nayak, S. Metal-organic frameworks as potential agents for extraction and delivery of pesticides and agrochemicals. *SC Omega* **2022**, *7*, 45910–45934.
89. Chen, M.-L.; Lu, T.-H.; Li, S.-S.; Wen, L.; Xu, Z.; Cheng, Y.-H. Photocatalytic degradation of imidacloprid by optimized Bi_2WO_6/NH_2-MIL-88B(Fe) composite under visible light. *Environ. Sci. Pollut. Res.* **2022**, *29*, 19583–19593. [CrossRef] [PubMed]
90. Yang, Y.; Ma, X.; Yang, C.; Wang, Y.; Cheng, J.; Zhao, J.; Dong, X.; Zhang, Q. Eco-friendly and acid-resistant magnetic porous carbon derived from ZIF-67 and corn stalk waste for effective removal of imidacloprid and thiamethoxam from water. *Chem. Eng. J.* **2022**, *430*, 132999. [CrossRef]
91. Chen, M.-L.; Lu, T.-H.; Long, L.-L.; Xu, Z.; Ding, L.; Chen, Y.-H. NH_2-Fe-MILs for effective adsorption and Fenton-like degradation of imidacloprid: Removal performance and mechanism investigation. *Environ. Eng Res.* **2021**, *27*, 200702. [CrossRef]